Nuclear Science & Technology Research Institute

Journal of Nuclear Research and Applications

Research Paper

Journal homepage: https://jonra.nstri.ir

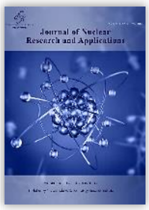

Benchmark Study of Simulations of Silicon-Equivalent Aluminum Phantom Using Thermal Neutron Flux Measurements at Some Irradiation Positions in Tehran Research Reactor

Z. Gholamzadeh*[1], H. Jafai[2], M. Kardan[1], A. Ezati[1], M. Dastjerdi[2]

[1] *Reactor and Nuclear Safety Research School, Nuclear Science and Technology Research Institute (NATRI), P.O.BOX: 14395-836, Tehran, Iran.*
[2] *Nuclear Engineering Faculty, Shahid Beheshti University, P.O.BOX: 19839-4716, Tehran, Iran.*

(Received: 24 July 2024, Revised: 25 November 2024, Accepted: 25 November 2024)

A B S T R A C T

In semiconductor production, doping is the intentional introduction of impurities into an intrinsic semiconductor to modulating its electrical, optical, and structural properties. Among various areas of research reactor utilization, neutron transmutation doping of silicon is a well-established technology desired by industry. The design and construction of an irradiation channel require calculations and benchmark studies to validate the calculations performed. This work is based on the measurement of thermal neutron flux inside an 8-inch aluminum phantom using gold foils positioned radially inside it. The irradiation positions were simulated using the MCNPX computational code to investigate the conformity of the code data with the experimental data. The results showed noticeable discrepancies between the measured data inside the TRR thermal column and the obtained simulation data obtained. These differences may be due to some physical properties of the thermal column nose that need to be properly considered for precise simulation of the irradiation conditions. While benchmark study for the other selected irradiation position near the TRR core showed an average 25% relative discrepancy between the simulation and experimental data. The simulations carried out inside an optimized irradiation channel designed for 6-inch silicon ingots showed that have a thermal neutron flux of at least in order of 1012 would be achievable. This makes it possible to complete the doping process in 2 to 3 days of operation of the TRR reactor at its full 5 MW power.

Keywords: *Neutron transmutation silicon doping; Thermal neutron flux; Aluminum phantom*.

1. Introductions

In semiconductor production, doping is the intentional introduction of impurities into an intrinsic semiconductor. Neutron transmutation doping (NTD) is an unusual doping method used for special applications. It is most commonly, used to dope silicon n-type in

*Corresponding Author E-mail: cadmium_109@yahoo.com
DOI: https://doi.org/10.24200/jonra.2024.1622.1131.

high-power electronics and semiconductor detectors [1-2]. Boron, arsenic, phosphorus, and occasionally gallium are used to dope silicon. Boron is the preffered p-type dopant for silicon integrated circuit production because it diffuses at a rate that allows for easily controllable junction depth. For example, common doping techniques for N-type silicon wafers include the diffusion of phosphine gas. The usual doping methods are chemical, and p-type doping is not possible using research reactors [3]. However, the possibility of smoothly doping silicon using research reactors has made this process a valuable method for producing high-quality doped n-type crystals.

Since 1970, NTD of silicon has been gradually utilized for the production of silicon with uniform for power device fabrication. The idea of producing semiconductors with perfectly dopant distribution by NTD was originally described by Lark-Horvitz at 1951 [4].

The NTD process occurs when undoped (high-purity) silicon is irradiated in a thermal neutron flux. The thermal neutron is captured by the 30Si atom, which has a 3% abundance in pure Si. The silicon's transmutation by neutrons to phosphorus decreases the sample's resistivity [5].

The NDT process happens as the following equation:

$$ {}_{14}Si^{30} + n = {}_{14}Si^{31} - \beta^{-1}(2.62h) \rightarrow {}_{15}P^{31} \qquad (1)$$

The interest in NTD has two main advantages over other methods of impurity incorporation. First, it offers high-precision doping, because the concentration of impurities is introduced at a constant neutron flux and can be controlled with high accuracy. The second advantage is the high homogeneity of impurity distribution [6].

One of the important basic parameters in silicon doping is the ratio of thermal to fast neutron flux. This process must be carried out where the thermal neutron flux is considerably higher than the fast neutron flux. The IAEA recommends that the thermal to fast neutron flux ratio should be at least 7:1 [7].

Fast neutron induced defects result from the displacements of silicon atoms from their normal lattice positions primarily through elastic collisions and recoils caused by the emission of β and γ rays. Lattice displacements are unfavorable and should be minimized [8].

The irradiation of large diameter silicon ingot is being carried out more efficiently in heavy water research reactors. This is due to the fact that the thermal neutron flux to fast neutron flux ratio is typically around 1000:1. Additionally, neutron filters should be designed to moderate the neutrons and increase the thermal to fast neutron ratio [5].

The HANARO 30 MW heavy water-reflected research reactor routinely irradiates silicon ingots inside the irradiation channels installed in the heavy water reflector. The Silicon channels for the irradiation of ingots have diameters of 22 cm and 17 cm, with silicon crystals of 6 and 8 inches, as well as 5 and 6 inches, respectively, doped inside them. The thermal neutron flux is 3.7×10^{13} n/s.cm^2. The length of the ingot is 60 cm in of all cases. Four hours of irradiation of the ingots produces a resistivity of 50 Ω.cm [10]. The Silicon doping capacity at HANARO is 50 tons per year including 20 tons of 5 and 6-inch crystals [10]. It was reported in 2008 that HANARO can produce more than 50 tons of NTD-Si per year including 8-inch crystals as well [11].

MURR, a 10 MW swimming pool beryllium-reflectedreactor, utilizes a graphite outer reflector for irradiating silicon. Thermal fluxes are in the range of 1×10^{14} n/s.cm^2 in the core trap, 10^{13} range in the graphite reflector, 10^{12} range in the S-basket (Fig.1) used for silicon doping and 10^{11} in the variable flux facility [12].

All reactors that produce NTD silicon rotate the silicon ingots improve radial wafer uniformity. Radial uniformity across wafer diameters of 3 inches or less is typically no more than ±1% for 50 to 100 Ω-cm material unless extreme radial non-uniformities existed in the starting material. The rotation speed is 1.9 rpm at the MURR facility [12].

Table 1 presents the most important research reactors that are used for doping silicon ingots commercially [7].

In order to design an irradiation channel for silicon doping, theoretical calculations using computational codes must be validated through experimental measurements. The self-powered neutron detector (SPND) is typically used for flux monitoring. However, when the irradiation time is not long enough to ignore the response time of the SPND, dynamic compensation of SPND signals may be necessary. Since the SPND can only be located outside of the ingot, its signal must be calibrated to the neutron flux within the ingot. This can be achieved by attaching neutron activation foils or wires in between ingots. However, the calibration factor may vary depending on factors such as geometrical core configuration, control rod position, fuel burn up, SPND burn up, etc [7].

Because the neutron absorption cross section siliconof is close to that of aluminum, it is possible to observe the behavior of neutron flux in silicon ingots by using an aluminum phantom. Gold foils can be placed in radial and axial directions inside it (Fig. 2).

Some theoretical calculations have been conducted to design a silicon doping irradiation channel in the Tehran Research Reactor (TRR) [14].

Another published work has shown that the TRR thermal column has great potential for installing silicon doping channels. Especially at a position 90 cm away from the core center, the thermal neutron flux and the ratio of thermal to fast neutron flux in the optimal location are 1.2×10^{12} n/s.cm^2 and 441, respectively. It should be noted the values are very tightly depended to the graphite material density used inside the thermal column as well as its integrity when the graphite boxes are filled inside the aluminum structure of the thermal column nose [15].

The present study aims to benchmark the simulations with experimental measurements using an aluminum phantom.

2. Material and Methods

The Tehran Research Reactor is an open pooltype reactor with a light-water moderator and coolant, generating 5 MW thermal power, which is used for research, educational, and radioisotope production purposes. Fig. 3 shows the layout of the reactor [16].

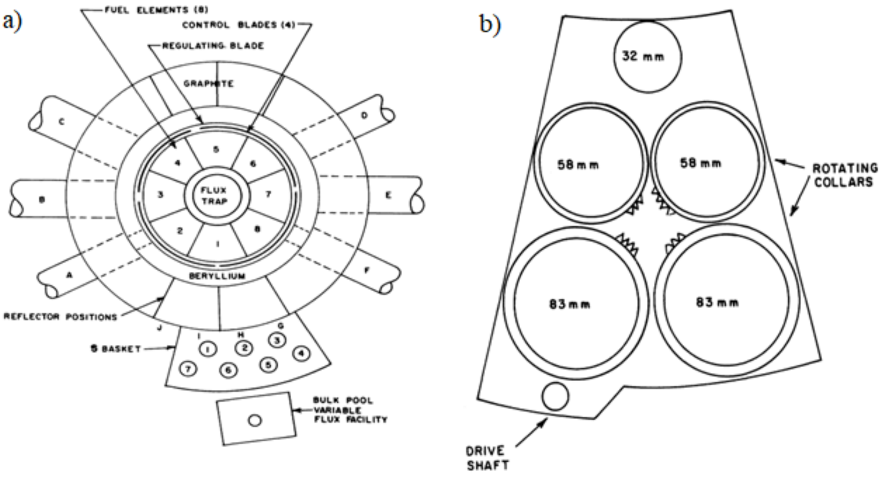

Fig. 1. University of Missouri Research Reactor, MURR a) Cross-sectional view b) The silicon irradiation wedge located in the graphite reflector [12].

Table 1. Reactors in production or silicon doping research [7].

Reactor name	Country	Power (MW)	Thermal neutron flux (n/s.cm²)	Thermal/fast neutron flux (n/s.cm²)	Irradiation location and commercial production capacity
MITR-II	USA	5	5.5×10^{12} -2.5×10^{12}		Radial canals above core
MURR	USA	10	6.0×10^{14}	6	
IRT-T	Russian Federation	6	2×10^{13}		Radial canals above core
JEEP II	Norway	2	9×10^{12} -4×10^{12}		Channel inside the core reflector (4 ton/y)
HFR	Netherlands	45	2.5×10^{13}		Beryllium intra reflector channel
MARIA	Poland	30	2.1×10^{13}	50	The channel inside the graphite reflector (9 ton/y)
OPAL	Australia	20	1.6×10^{13} - 1.7×10^{12}	900	The channel inside the core reflector (20 ton/y)
FRMII	Germany	20	1.6×10^{13}	1700	Heavy water tank near the core (8 ton/y)
BR2	Belgium	100	5.3×10^{13}	5.3	Inside the beryllium channel near the core (15 ton/y)
SAFARI-1	South Africa	20	1.5×10^{14}	5.76	next to the core (20 ton/y)
HWRR-II	China	15	2.4×10^{12}		Intra reflective channels around the core
CARR	China	60	8×10^{14}	0.8	Heavy water tank near the core
MJTR	China	5	4.52×10^{13}	0.46	Inside the core and reflector (20 ton/y)
HFETR	China	125	4.2×10^{14} -1.2×10^{14}	0.48	Channel near the core
LVR-15	Czech	10	2.7×10^{13}	12.27	Channels behind the core reflector
IEA-R1	Brazil	5	7×10^{12}		Channel inside the graphite reflector around the core (1 ton/y)
OSIRIS	France	70	4×10^{13}	80	Channel inside the core reflector (10 ton/y)
ORPHEE	France	14	1×10^{13}	1000	The channel inside the heavy water tank (6 ton/y)
HANARO	Korea	30	5.2×10^{13}	400	Vertical channel in heavy water around the core (2.8 ton/y)

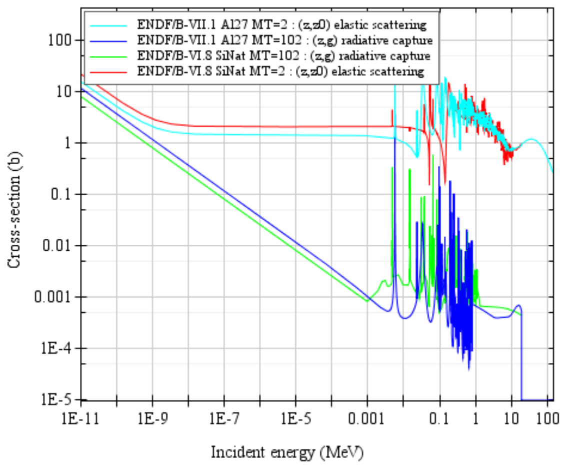

Fig. 2. Comparison aluminum and silicon neutron absorption and elastic scattering cross section [13].

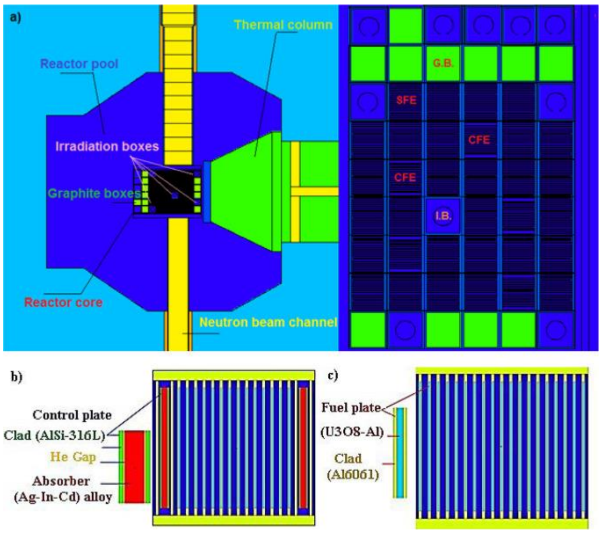

Fig. 3. Cross sectional view of a) the modeled TRR core b) SFE; standard fuel assembly c) CFE; control fuel assembly [16].

The fuel burnups were different which have been requested from the TRR fuel management operator, the values changing from 2.7% as the least-burnup assembly and 45.81% as the highest-burnup assembly. The coolant temperature was considered 300 K regarding the available and the closest temperature to the TRR operational condition.

The TRR and aluminum phantom irradiation position simulations were performed using the MCNPX2.7. MCNPX is a general-purpose Monte Carlo radiation transport code with multitasking capabilities that help reduce the time needed to obtain computational result [17]. The MCNPX code was developed during the last three decades at Los Alamos National Laboratory and can be considered ‘‘the state-of-the-art’’ Monte Carlo code. This code is capable of transporting 36 elementary particles at all energies, and its generalized geometry features and use of continuous-energy cross-sections allow for generating benchmark-quality results for various nuclear applications [18].

To measure neutron flux at two specific positions, an aluminum phantom with a 6-inch diameter (the same one selected for silicon ingots to be doped in TRR) and 30 cm height was constructed according to Fig.4. Several 8 mm holes were made inside the aluminum phantom following Fig.4.c. Fully fit aluminum rods with the appropriate hole diameters were made having gold foil loading capability shown in Figs. 4a and 4b. The phantom has made of aluminum 6061. Five holes were placed at middle plan of the phantom with 5.5 cm intervals and two holes were placed at the edges of the phantom (Fig.4b). T6 Heat Treated 6061-Cold Finish Aluminum Bar offers above average corrosion resistance, good machinability, high strength, light weight, good weldability and heat treatability for increased strength, all at a reasonable cost. 6061 is the most widely used aluminum alloy globally due to its favorable properties. Typically used in aerospace, automotive, cameras, couplings, marine hardware, electrical components, decorative hardware, structural applications, pins, brakes, pistons, valves, and bicycle frames. Its composition includes 98% Al, 0.35% Cr, 0.4% Cu, 0.8% Mg, and 0.45% Si.

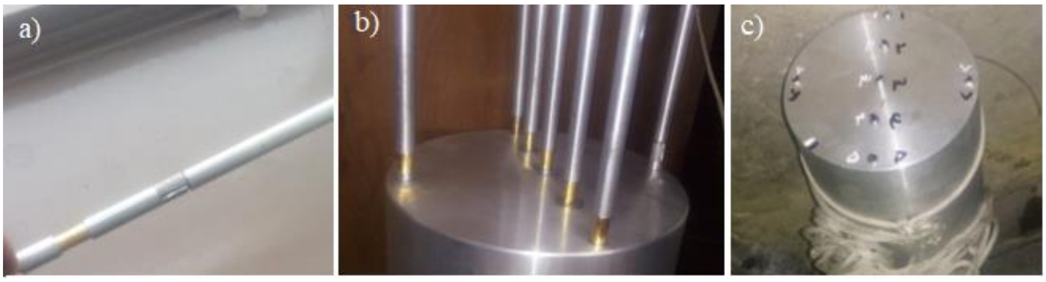

Fig. 4. Aluminum phantom of a) aluminum rod b) the rod loading inside the phantom c) the phantom full view.

To measure thermal fast neutron ratio, some 10 µm thick gold foils of 1×1 cm^2 were wrapped around the aluminum rod, completely bare, and others were wrapped with a 1 mm thick cadmium foil covered them. The gold foils and cadmium-covered one's special distances were planned so that no shadowing effect could not be used for flux measuring. This can be clearly observed in Fig.4a that the golden-colored is the wrapped gold foil and the silver-colored is the gold foil covered by the cadmium thermal neutron absorber. Thermal neutron flux is measured by the foil activation method. The activity is measured using an NaI gamma detector by counting the ^{198}Au decay rates at a finite time. The mass of the activated foil is measured using a high-precision digital scale. The following formula is used to determine experimental thermal neutron flux:

$$A = N\sigma\varphi(1-e^{-\lambda t}) \tag{2}$$

Where N represents the gold foil atoms (determined from the measured mass), σ is the absorption microscopic neutron cross-section, φ is the thermal neutron flux to be measured, A is the foil activity determined by the NaI detector, λ is the decay constant of ^{198}Au, and t is the time delayed after the foil is released from the reactor and foil counted by the gamma detector.

Fast neutron flux, which is considered to be above 0.5 MeV in this work, is measured using cadmium-covered gold foil counting by NaI. The counts from the previous foil minus the cadmium-covered one determine the fast section of the neutron spectra exposed to the foils. The same formula is used to calculate the fast neutron flux.

In the simulations the neutron spectra and determination of thermal and fast neutron quotas are calculated using the F4 tally card of MCNPX. The fluxes inside the gold foil volumes are calculated in KCODE mode of the MCNPX code. The energy card is used along with the F4 tally card to calculate the neutron fluxes at different energy groups (En< 0.5 MeV and En>0.5 MeV).

To determine the particle flux into a volume, the F4 tally can be employed. If a particle of weight W and energy E travels a track-length (segment) T within a specified cell of volume V, this segment makes a contributes WT/V to the flux (fluence) in the cell. The sum of these contributions is reported as the F4 tally in the MCNP output. Technically, if Φ(r, E, Ω) represents the energy and angular distribution of the fluence as a function of position, the F4 tallies would measure [19]:

$$F4 = \frac{1}{V}\int_V dV \int_E dE \int_{4\pi} d\Omega\,\Phi(r,E,\Omega) \quad \left(\frac{\frac{n}{cm^2}}{\text{source particle}}\right) \tag{3}$$

Two positions were considered for the irradiation of the gold foils loaded inside the aluminum phantom to monitor the radial thermal neutron flux at the mid-plane of the phantom. The first position is the end of the TRR thermal column nose, which provides access for sample loading. The irradiation conditions were simulated using the MCNPX code asshown in Fig.5. Do to the arrangement of graphite blocks of measuring 10×10×30 cm³ inside the thermal column nose, there is a lack of integrity of the graphite material inside the nose as depicted in Fig. 5.

The impact of this lack of integrity on the measurement was discussed and investigated considering the assumption of air or water between the graphite blocks. Hence, further simulations were carried out regarding 5 mm gap between the graphite blocks installed inside the thermal column nose shown in to Fig. 6.

Since the core of the TRR is occasionally transferred to the second pool and then returned to the first pool, it was assumed that it has shifted about 2 cm from its original location, and therefore the distance between the lead piece of the thermal column nose and the edge of the grid plate increased to 4 cm. Then, the effect of having 4 cm of water between the thermal column nose and the lead piece on the calculated amount of thermal neutron flux was investigated. This was done by placing gold foils inside the aluminum phantom under the radiation within the thermal column as shown in Fig. 7.

During the fuel management of the TRR, changes may be made to the arrangement of the reactor core or its reflectors. The next step involved investigating the effect of these changes on the thermal neutron flux calculations of the gold foils loaded in the aluminum phantom (Fig. 8).

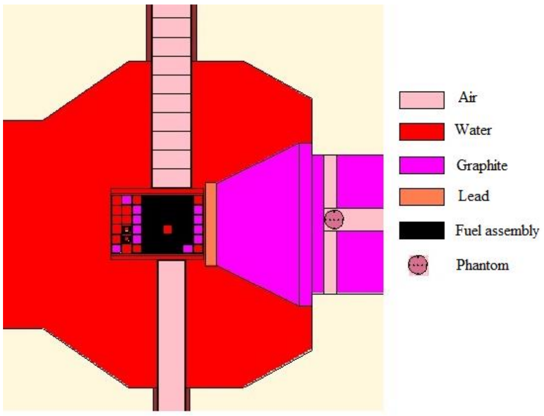

Fig. 5. Simulation of the aluminum phantom inside the TRR thermal column behind the graphite nose.

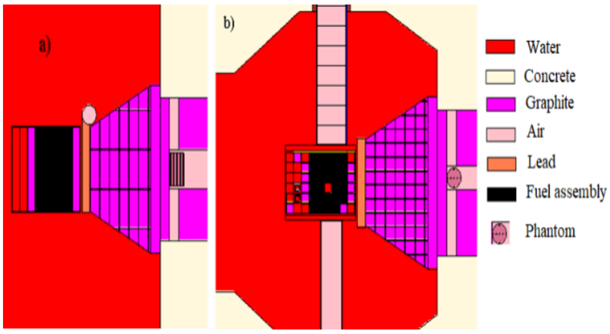

Fig. 6. Simulation of lack of integrity for graphite nose of TRR thermal column.

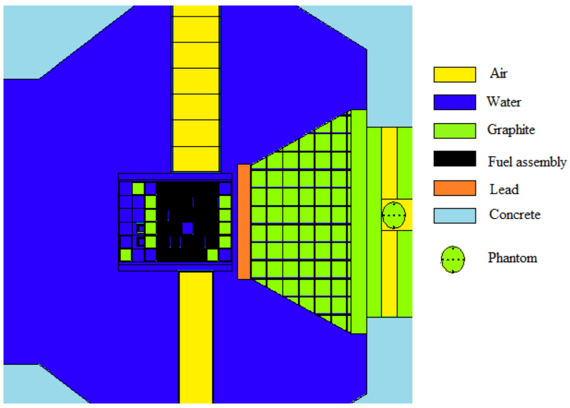

Fig. 7. Investigation of TRR core grid plate displacement effect on the calculated neutron flux inside the simulated phantom.

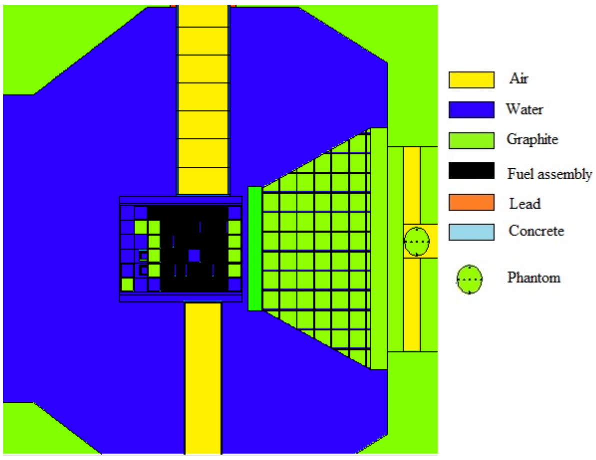

Fig. 8. Investigating the partially change of the arrangement of TRR core on the thermal neutron flux inside the simulated phantom.

For a benchmark study comparing simulations to measurements, another irradiation position of the aluminum phantom was selected near the TRR core. The irradiation conditions were simulated using the MCNPX code shown in Fig. 9. The aluminum phantom was placed on the grid plate surface, facingthe 30 cm end length of the TRR fuel assemblies. Fine tuning of the Phenom was not possible as it was manually adjusted approximately 7 meters below the TRR water biological shield. However, its positional displacement was less than 2 cm.

Finally, an aluminum phantom was modeled inside the graphite nose of the thermal column to investigate the thermal neutron flux inside the phantom at the optimized suggested position according to ref.15 which was 90 cm away from the core center where the silicon ingot is going to be doped (see Fig. 10).

3. Result and Discussion

The calculations presented in Table 2 show that the radial thermal neutron flux data is approximately 65 times higher than the measured values. These calculations took into account the integration of the thermal column nose as shown in Fig. 5.

A high discrepancy between the previous thermal neutron fluxes could be the result of using 10×10×30 cm^3 graphite blocks inside the thermal column nose, which disturbs the material integrity shown in Fig. 5. Therefore, in the next step a 5 mm gap was considered between the graphite blocks as a worst-case scenario, since condition because in reality the gap may be less than the selected value. The calculations carried out showed that if air has filled the gap, the radial thermal neutron flux data is about 119 times higher than the measured values (Table 3). Clearly, reducing the absorber graphite material would result in such increase.

The calculations carriedout showed that if water has filled the gap, the radial thermal neutron flux data is about 13 times higher than the measured ones (Table 4). The Water penetration inside the part is completely possible, because of its aging.

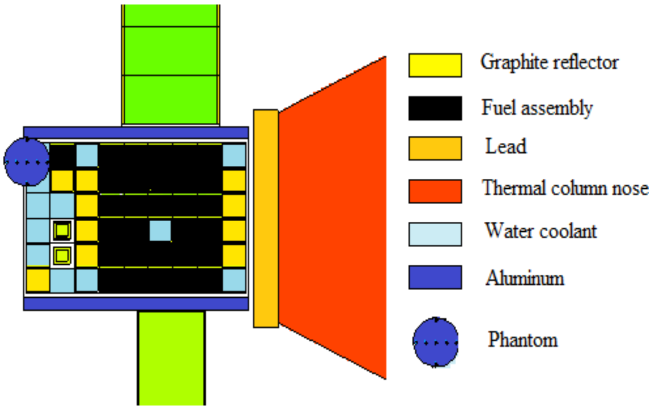

Fig. 9. Aluminum phantom simulation near TRR core.

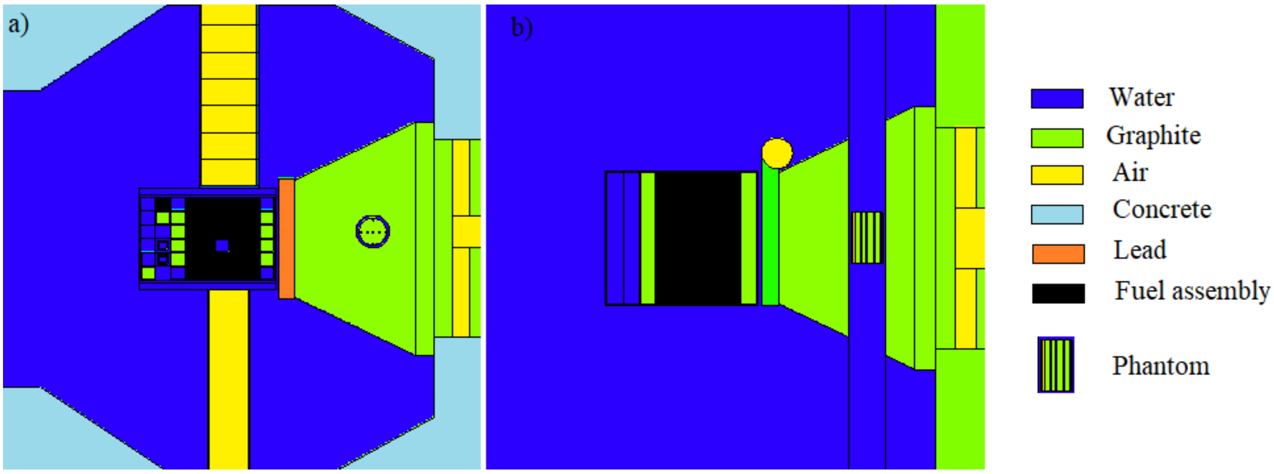

Fig. 10. Aluminum phantom simulation inside TRR thermal column nose (a channel located at 90 cm from the core center).

Table 2. Comparison of radial thermal neutron flux measured using gold foils and calculated using MCNPX code when the aluminum phantom is placed inside thermal column, material integrity was considered for the thermal column nose.

Foil number	Measured neutron flux ×10⁹ (n/cm².s)	Calculated neutron flux ×10¹¹ (n/cm².s)
1	3.38	2.14
2	3.15	1.85
3	2.80	1.79
4	2.28	1.63
5	2.19	1.53

Table 3. Comparison of radial thermal neutron flux measured using gold foils and calculated using MCNPX code when the aluminum phantom is placed inside thermal column, disintegrated-material with air gaps was considered for the thermal column nose.

Foil number	Measured neutron flux $\times 10^{9}$ (n/cm^2.s)	Calculated neutron flux $\times 10^{11}$ (n/cm^2.s)
1	3.38	3.96
2	3.15	3.62
3	2.80	3.00
4	2.28	2.94
5	2.19	2.77

The Water penetration trough the graphite part was proved as TRR pool water evacuation or recharge some bubbles that are observed on top of the thermal column nose. Clearly when the pool water is evacuated the pressure differences causes some penetrated water be ejected outside of the graphite part and during the pool water filling the reverse phenomena is happened.

Table 4. Comparison of radial thermal neutron flux measured using gold foils and calculated using MCNPX code when the aluminum phantom is placed inside thermal, disintegrated-material with water gaps was considered for the thermal column nose.

Foil number	Measured neutron flux $\times 10^{9}$ (n/cm^2.s)	Calculated neutron flux $\times 10^{10}$ (n/cm^2.s)
1	3.38	4.10
2	3.15	3.82
3	2.80	3.51
4	2.28	3.42
5	2.19	3.28

Another possible change that may create such discrepancy between the simulation and experimental data is the core gird plate has a displacement from the TRR thermal column nose. Hence, a 2 cm displacement was modeled using MCNPX code according to Fig. 7. The carried-out calculations showed if water has filled the gap, and there is a 2 cm displacement, the radial thermal neutron flux data is about 5 times higher than the measured ones (Table 5).

The TRR core configuration is changed at different fuel cycles and fuel managements The discrepancy between the measured values and the calculated ones was discussed for a different core configuration than one mentioned above as it was modeled according to Fig. 8. The calculations showed that if water has filled the gap between the graphite blocks of the thermal column nose, and there is a 2 cm displacement of the grid-plate (the same simulation condition as in Table 4), the radial thermal neutron flux data simulated using the MCNPX code is about 15% different than the previously calculated data (Table 6). Therefore, the TRR core configuration may change neutron flux up a few ten percent.

Graphite brittleness and damage are other possible reasons for the discrepancy between the experimental and theoretical thermal neutron flux data. The observed high discrepancy caused the experimental and simulation of the aluminum phantom to be carried out beside the TRR core according to Fig. 9.

Table 5. Comparison of the radial thermal neutron flux measured using gold foils and calculated using MCNPX code when the aluminum phantom is placed inside the thermal column, disintegrated-material with water gaps was considered for the thermal column nose as well as 2 cm grid-plate displacement.

Foil number	Measured neutron flux×10^9(n/cm^2.s)	Calculated neutron flux×10^{10}(n/cm^2.s)
1	3.38	1.73
2	3.15	1.53
3	2.80	1.36
4	2.28	1.27
5	2.19	1.23

The carried-out calculations showed a radial neutron flux inside the phantom near the core in order of 10^{12} n/s.cm^2, with its average value of 3.1×10^{12} n/s.cm^2 inside the aluminum phantom. The value is 2.5×10^{12} n/s.cm^2 according to the radial measured data. The experimental radial thermal neutron flux peaking factor is 1.63 according to the experimental data obtained from the activated gold foils inside the aluminum phantom near the core. The value is 1.82 according to the simulation data. There is a 25% relative discrepancy between the measured and calculated thermal neutron flux data (Fig. 11).

Table 6. Comparison of radial thermal neutron flux measured using gold foils and calculated using MCNPX code when the aluminum phantom is placed inside the thermal column, disintegrated-material with water gaps was considered for the thermal column nose and 2 cm grid-plate displacement as well as TRR core configuration change.

Foil number	Measured neutron flux×10^9(n/cm^2.s)	Calculated neutron flux×10^{10}(n/cm^2.s)
1	3.38	2.03
2	3.15	1.69
3	2.80	1.64
4	2.28	1.51
5	2.19	1.38

To design a silicon-doping channel for TRR inside its thermal column nose, the design and construction of the reflector part and the irradiation channel inside it should be carried out to be replaced with the available one as shown in Fig. 10. The channel design and optimization have been performed according to ref.17 to load the 8-inch silicon ingots. The best position is a channel located 90 cm away from the TRR core center. The aluminum phantom was modeled inside the channel to calculate the thermal neutron flux at the gold foils' position inside the phantom.

The carried-out calculations showed that the radial neutron flux inside the optimized channel is in order of 10^{12} n/s.cm^2, with its average value of 1.2×10^{12} n/s.cm^2 over the aluminum phantom. The radial peaking of thermal neutron flux is 1.74 according to the simulation data observed in Fig. 12.

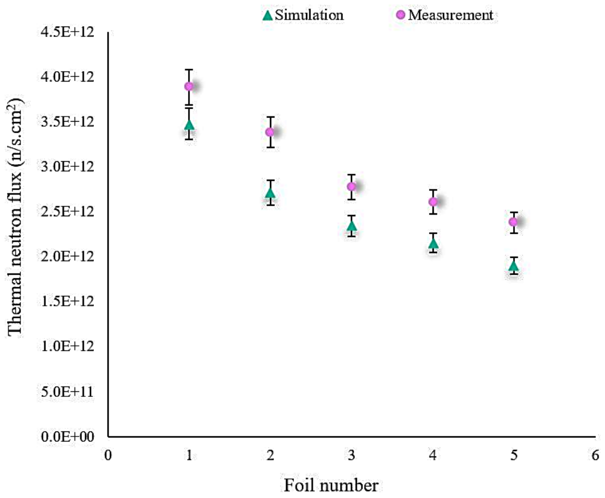

Fig. 11. Comparison of thermal neutron flux inside the radial inserted gold foils in the aluminum phantom located near the TRR core and the measured values.

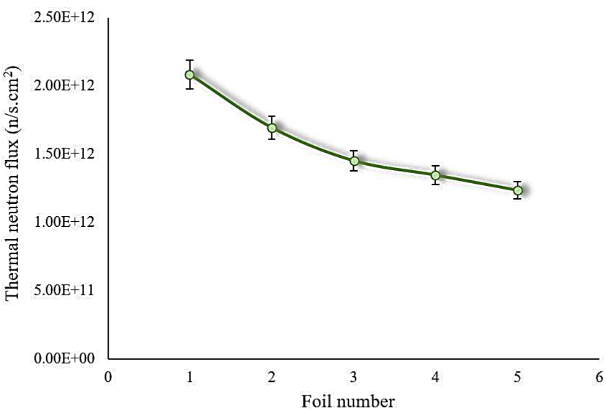

Fig. 12. Calculation of thermal neutron flux inside the radial-inserted gold foils in the aluminum phantom located at 90 cm from the TRR core center.

The radial peaking of the thermal neutron flux is 1.82 according to the theoretical data observed in Fig. 12. Gamma-deposited heat inside the phantom are 41.66 W and neutron-deposited heat is 0.21 W. Thermal to fast neutron flux ratio is 62.1 for fast neutrons with En>0.18 MeV and 147 for fast neutrons with En>1 MeV.

In addition, the calculations showed that the average thermal neutron flux would be 13% higher in silicon ingot than the aluminum phantom because of its higher scattering to absorption cross sections.

Whereas the TRR FSAR has not been updated over the last 7 years, only the D6 thermal neutron flux of the equilibrium core in the reported FSAR was compared with the simulated value in this work. It should be mentioned the TRR operation condition could change some neutronic parameters, especially at the core borders which are affected by for example topaz loading and so on. To test the accuracy of the program used, the thermal neutron flux in the radiation boxes of the equilibrium core used in this study was calculated and compared with the value mentioned in the FSAR of the TRR [20]. The results of the calculations showed that the thermal neutron flux calculated in the D6 channel was 1.13×10^{13} n/s.cm^2 and the value is 1.77×10^{13} n/s.cm^2 in the FSAR. The effective multiplication factor of the equilibrium core modeled in this work at the beginning of the cycle (BOC) is 1.03085 and the value reported in FSAR at the beginning of the cycle (BOC) is 1.03131. It is necessary to mention that the difference between the calculation values of this code and FSAR is in the order of calculation error.

4. Conclusion

Neutron transmutation doping (NTD) of semiconductor materials is a method in which the quantity of dopant can be precisely controlled and homogeneously distributed throughout the material. This method is widely used by many research reactors to create free electrons and low resistivity. It not only provides direct commercial income for nuclear research reactors but also helps develop the power-device industry. This research focuses on thermal neutron flux monitoring using an aluminum phantom that can be approximated as a silicon ingot due to their similarities for neutron absorption cross sections. The experimental neutron flux monitoring helps the irradiation channel design and construction be validated by comparison with the simulation data and also the expensive silicon ingot doping achieved the best-predicted irradiation conditions. The present simulations showed the thermal column room is not suitable for silicon doping because of its low thermal neutron flux in the order of 10^{11} n/s.cm^2. Experimental tests at this position showed a high discrepancy with the carried-out simulations. Theoretically, investigations showed water penetration inside the installed graphite nose of the thermal column inside the TRR pool may resulted in this high discrepancy. The TRR operator verified the occurrence as the part aging phenomena during 50-years TRR operation while bubble formation has been observed top of it during the pool water evacuating and filling. The equivalent phantom with silicon ingot was placed near the core edge to validate the simulation result with the experimental neutron flux monitoring which is going to be done using gold foils inside it. The results showed a very good agreement between the simulation and measurements while the relative discrepancy was less than 25%. To further reduce this discrepancy, more detail simulation of the TRR core operation such as the precise burnup of the fuels, control rod positions, and evaluation of uncertainties like counting times of the foils, detector uncertainty, foil mass measuring uncertainty, and foil position displacement during irradiation, should be considered.

Conflict of interest

The authors declare no potential conflict of interest regarding the publication of this work.

References

[1] Łukasiak L, Jakubowski A. History of Semiconductors. Journal of telecommunications and information technology. 2010 Mar;39(1):3-9. doi:10.26636/jtit.2010.1.1015.

[2] Wilson A.H. The Theory of Metals (2nd ed.). Cambridge University Press. 1953. doi.:10.1119/1.1933705.

[3] The Complete Guide to Doping in Semiconductors. https://www.waferworld.com.

[4] Sheibani S, Moattar F, Ghannadi Maragheh M, Khalafi H. Investigation of a simple and efficient method for silicon neutron transmutation doping process in Tehran research reactor. Annals of Nuclear Energy. 2002 July;29(10):1195-1208. doi:10.1016/S0306-4549(01)00100-1.

[5] El Latif S.S.M. Design of Large Sample Silicon Ingots Irradiation Facilities Using MCNP. Master of Science thesis. 2012.

[6] Shlimak I.S. Neutron transmutation doping in semiconductors: science and applications. Physics of the Solid State. 1999 May;41(5):716-719. doi.:10.1134/1.1130856.

[7] Neutron Transmutation Doping of Silicon at Research Reactors. IAEA-TECDOC-1681. 2012.

[8] Osmani N, Benkharfia H, Saad D. Neutron-induced damage simulations using MCNP6 and SRIM codes: Beyond neutron transmutation doping of silicon. Annals of Nuclear Energy. 2023 July;187:109795. doi:10.1016/j.anucene.2023.109795.

[9] Kim H.S, Oh S.Y, Jun B.J, Kim M.S, Seo C.G, Kim H.I. Design of a neutron screen for 6-inch neutron transmutation doping in HANARO. Nuclear Engineering and Technology. 2006 Jan;38(7):675-680.

[10] Park S.J, Kang K.D, Kim M.S, Lim I.C. Neutron transmutation doping in HANARO reactor. IAEA-TM-38728. 2010.

[11] Park S.J, Lim I.C. Neutron Transmutation Doping of Silicon Crystal in HANARO, Conference: 2008 autumn meeting of the KNS. Pyongchang (Korea, Republic of). 2008 Oct;30-31.

[12] Meese J, Cowan D, Chandrasekhar M. A review of transmutation doping in silicon. IEEE Transactions on Nuclear Science. 1979 Dec;26(6):4857-4867. doi:10.1109/TNS.1979.4330241.

[13] EXFOR: Experimental Nuclear Reaction Data-IAEA-NDS. https://www-nds.iaea.org/exfor/servlet/E4sMakeE4.

[14] Heydari M, Jafari H, Gholamzadeh Z. Optimization study to determine the appropriate location for the implementation of silicon doping in Tehran research reactor. Radiation Physics and Engineering. 2023 Oct;4(4):7-14. doi: 10.22034/rpe.2023.385820. 1117.

[15] Kardan M, Gholamzadeh Z, Bavarnegin E, Jozvaziri A, Kasesaz Y, Ezati A, Sadeghi N, Alizadeh F. Feasibility study of silicon doping potential in Tehran research reactor thermal column. *Radiation Safety and Measurement.* 2021;9(1):43-54 [In Persian].

[16] Gholamzadeh Z, Bavarnegin E. Gamma and neutron dosimetry of Tehran Research Reactor containment during and after LOCA accident. Applied Radiation and Isotopes. 2019 Mar;145:59–67. doi: 10.1016/j.apradiso.2018.12.016.

[17] Pelowitz D.B. MCNPX User's manual version 2.6.0, LA-CP-07-1473. 2008.

[18] Aslani Menarebazari Z, Jafari H, Gholamzadeh Z. The design and construction of a collimator holder to equip beam tube D of the Tehran Research Reactor. Nuclear Engineering and Design. 2023 Apr;405:112226. doi:10.1016/j.nucengdes.2023. 112226.

[19] Shultis J.K, Faw R.E. An MCNP primer Dept. of Mechanical and Nuclear Engineering Kansas State University. Revised. 2008 July 21.

[20] Introduction and general description of research reactor. Basic Equilibrium Core. FSAR of Tehran Research Reactor. P:40 (TRR-SA- RPT- 052) [In Persian].

How to cite this article
Z. Gholamzadeh, H. Jafai, M. Kardan, A. Ezati, M. Dastjerdi. *Benchmark Study of Simulations of Silicon-Equivalent Aluminum Phantom Using Thermal Neutron Flux Measurements at Some Irradiation Positions in Tehran Research Reactor*. Journal of Nuclear Research and Applications (JONRA), Volume 5 Number 1 Winter (2025) 43-55, **URL:** https://jonra.nstri.ir/article_1698.html, **DOI:** https://doi.org/10.24200/jonra.2024.1622.1131.